*macromol*

MDPI

*Article*

# Structural Characteristics and Improved Thermal Stability of HDPE/Calcium Pimelate Nanocomposites

**Christina Samiotaki [1], Evangelia Tarani [2], Dimitra Karavasili [1], Alexandra Zamboulis [1], Konstantinos Chrissafis [2] and Dimitrios N. Bikiaris [1,*]**

[1] Laboratory of Chemistry and Technology of Polymers and Dyes, Department of Chemistry, Aristotle University of Thessaloniki, 54124 Thessaloniki, Greece; christinasamiotaki@gmail.com (C.S.); dkaravasil@chem.auth.gr (D.K.); azampouli@chem.auth.gr (A.Z.)

[2] Laboratory of Advanced Materials and Devices, Department of Physics, Aristotle University of Thessaloniki, 54124 Thessaloniki, Greece; etarani@physics.auth.gr (E.T.); hrisafis@physics.auth.gr (K.C.)

* Correspondence: dbic@chem.auth.gr

**Abstract:** In the present research work, calcium pimelate (CaPim) was synthesized and investigated as an additive for high-density polyethylene (HDPE). HDPE/CaPim nanocomposites were prepared by melt-mixing, with CaPim content ranging from 0.1% to 1%, affording white homogeneous materials. The chemical structure of the nanocomposites and the incorporation of CaPim was confirmed by infrared spectroscopy. The surficial morphology and the additive distribution were examined by scanning electron microscopy. Differential scanning calorimetry and X-ray diffraction measurements showed that the thermal transitions and crystal structure of HDPE are not affected by the incorporation of CaPim, while the mechanical properties are retained overall. This study focuses on the thermal degradation of HDPE nanocomposites, investigating the degradation mechanism and kinetic parameters through various analytical methods. Isoconversional techniques, including the Friedman method, Vyazovkin analysis, and Ozawa Flynn Wall analysis, were employed to calculate activation energies ($E_\alpha$). The degradation mechanism and kinetic triplet were determined based on a multivariate non-linear regression method (model-fitting). Finally, the presence of a CaPim additive was shown to increase the $E_\alpha$ of thermal degradation, consistent with the calculated dependence of $E_\alpha$ on the degree of conversion and the improved thermal stability of the HDPE matrix.

**Keywords:** HDPE; calcium pimelate; nanocomposites; thermal stability; isoconversional methods; thermal degradation kinetics



**Citation:** Samiotaki, C.; Tarani, E.; Karavasili, D.; Zamboulis, A.; Chrissafis, K.; Bikiaris, D.N. Structural Characteristics and Improved Thermal Stability of HDPE/Calcium Pimelate Nanocomposites. *Macromol* **2024**, *4*, 42–57. https://doi.org/10.3390/macromol4010003

Academic Editor: Andrea Sorrentino

Received: 3 January 2024
Revised: 28 January 2024
Accepted: 31 January 2024
Published: 5 February 2024



## 1. Introduction

High-density polyethylene (HDPE) is one of the most widely used thermoplastics, due to its inexpensive, lightweight, and durable nature. Its superior processing properties, along with its chemical resistance, flexibility, and bio-neutrality, allow it to be used for a variety of applications, such as bottles, food containers, household goods, housewares, toys, crates and pails, gas tanks for automotive use, etc. Furthermore, HDPE films are often used as bags and garbage bags in supermarkets [1,2]. HDPE consists of a backbone of $sp^3$ carbon atoms bonded to hydrogen atoms and is probably the simplest polymer in terms of molecular structure. Thus, not surprisingly, from a kinetic point of view, HDPE is one of the fastest polymers to crystallize from the melt to a solid state [3–5]. Indeed, nucleation, chain folding, and crystal growth occur easily at temperatures below the melting point [6]. HDPE optical, mechanical, thermal, and chemical properties are significantly affected by the crystallization process [7].

A wide variety of additives and nanofillers have been studied for HDPE and polyolefins in general, such as inorganic salts and oxides, silicas, clays, fibers, graphene, carbon nanotubes, etc. [8–14]. Depending on their nature, the fillers can contribute to improving the mechanical, thermal, optical, magnetic, electrical, and surface wear properties [15].

It is well-known that fillers, especially at the nanometric scale, can act as heterogeneous nucleation agents in the polymer matrix, and affect the crystallinity, spherulite size, and crystal orientation, with further effects on the final polymer properties [16].

Calcium pimelate (CaPim) is an interesting filler that has been developed as a highly effective and thermally stable β-nucleating agent (β-NA), i.e., a dispersed material that acts as a local nucleus and promotes heterogeneous nucleation [6,16,17]. CaPim is frequently used in isotactic polypropylene, inducing the formation of β-crystals, which are thermodynamically difficult to obtain without the presence of a nucleating agent, while providing a polymer with superior toughness [18]. CaPim has also been combined with other fillers to further magnify its results [19]. For example, with graphene, leading improved dispersibility in the PP matrix and thus higher nucleation ability [20], or it acts as a supportive material on $TiO_2$ to promote the degradation of the material [21].

In this context, the present study aims to examine the effects of incorporating small amounts of CaPim to HDPE. Calcium carbonate has been frequently used [22–24], but CaPim has been much less studied. Due to the pimelic ion, a higher affinity is expected with the polyethylene matrix. Compared to PP and due to the faster rate of crystallization of HDPE, it is difficult to control nucleation in HDPE; the impact of CaPim on the properties of HDPE is considerably less documented [6]. In the present work, CaPim was synthesized and investigated as an additive for HDPE. HDPE/CaPim nanocomposites containing 0.1%, 0.2%, 0.5%, and 1 wt% of CaPim were prepared via melt-mixing, resulting in materials distinguished by their consistent and clearly visible white appearance, indicating a comprehensive homogenization of the nanocomposite constituents. The materials were characterized via infrared spectroscopy regarding their chemical structure, their morphology was examined by scanning electron microscopy (SEM), and their crystallinity was assessed by X-ray diffraction (XRD). Thermal properties were studied by differential scanning calorimetry (DSC) and thermogravimetric analysis (TGA), while tensile tests were performed to assess their mechanical behavior.

## 2. Materials and Methods

### *2.1. Materials and Reagents*

For CaPim synthesis, calcium hydroxide ($Ca(OH)_2$) 95% and pimelic acid 98% were supplied by Alfa Aesar (Haverhill, MA, USA). For the nanocomposite preparation, HDPE LITEN MB 71 (MFR (190/2, 16): 8 g/10 min) was kindly donated by SILON s.r.o. (Sezimovo Ústí-Planá nad Lužnicí, Czech Republic).

### *2.2. Calcium Pimelate Synthesis*

CaPim, $Ca(O_2C(CH_2)_5CO_2)$, was prepared by the neutralization of pimelic acid with calcium hydroxide [18]. An amount of 3.2 g (20 mmol) of pimelic acid (PA) was dissolved in 20 mL of deionized water and an equimolar amount of calcium hydroxide ($Ca(OH)_2$) was added (aqueous suspension, 4 mmol/mL). The reacting mixture was left at 40 °C under stirring for 24 h. The formation of a white precipitate was observed. The final product was separated via filtration, washed with deionized water, and dried in an oven at 60 °C under vacuum. The yield was 78%.

### *2.3. Preparation of the Nanocomposites*

Both the HDPE and the synthesized CaPim were dried in an oven at 60 °C under vacuum overnight in order to remove any traces of humidity. The mixture was compounded in a Haake–Buchler reomixer (model 600) (Haake–Buchler Instruments Ltd., Saddle Brooke, NJ, USA) fitted with roller blades and a mixing head of 69 $cm^3$. Melt-mixing was carried out at 190 °C for 20 min. The prepared nanocomposites are listed in the following table (Table 1).

**Table 1.** Formulations of HDPE/CaPim nanocomposites.

| Sample | HDPE % (*w*/*w*) | CaPim % (*w*/*w*) | MFI (g/10 min) |
|---|---|---|---|
| CaPim 0 | 100 | 0 | 6.3 |
| CaPim 0.1 | 99.9 | 0.1 | 15.5 |
| CaPim 0.2 | 99.8 | 0.2 | 19.3 |
| CaPim 0.5 | 99.5 | 0.5 | 19.8 |
| CaPim 1 | 99 | 1 | 29.4 |

### *2.4. Characterization Methods*

#### 2.4.1. Dynamic Light Scattering (DLS)

DLS was used to evaluate the size of the CaPim particles with the Litesizer 500 particle analyzer (Anton Paar, Graz, Austria). Prior to analysis, a 10 µL sample of CaPim suspension was dispersed in 990 µL of water and sonicated for 5 min. All measurements were performed in triplicate.

#### 2.4.2. Melt Flow Index (MFI)

The melt flow indexes of neat HDPE and composite melts were measured at 190 °C, with a 2.16 kg load according to the ASTM standard D 1238-04 [25] and ISO standard 1133 [26]. A CEAST's Melt Flow Quick Index meter was utilized (CEAST, Turin, Italy).

#### 2.4.3. Scanning Electron Microscopy (SEM)

Specimens of the composites were prepared, carbon coated to provide good conductivity, and examined utilizing a JEOL JMS 7610 F (Jeol, Freising, Germany) scanning electron microscope, operating at 10 kV and fitted with an energy dispersive X-ray (EDX) Oxford ISIS 300 micro-analytical system (Oxford instruments, Abingdon, UK). Operational parameters included an accelerating voltage of 20 kV, a probe current of 45 nA, and a counting time of 60 s.

#### 2.4.4. Fourier Transform Infrared Spectroscopy (FTIR)—Attenuated Total Reflectance (ATR)

FTIR spectra were recorded on an FTIR-2000, Perkin Elmer, Waltham, MA, USA. An appropriate amount of sample was grinded with potassium bromide (KBr) and disks were further formed using a hydraulic press; 32 co-added scans were recorded from 4000 to 450 $cm^{-1}$, at a 4 $cm^{-1}$ resolution.

ATR spectra were recorded on an IRTracer-100 (Shimadzu, Kyoto, Japan) fitted with a QATR™ 10 Single-Reflection ATR Accessory (Shimadzu, Kyoto, Japan) with a diamond crystal, and 16 co-added scans were collected from 450 to 4000 $cm^{-1}$ at a resolution of 2 $cm^{-1}$. Spectra were converted in absorbance mode.

The baseline of all presented spectra was corrected, and spectra were normalized.

#### 2.4.5. Differential Scanning Calorimetry (DSC)

Composite materials were analyzed with a Perkin Elmer Pyris Diamond differential scanning calorimeter (Solingen, Germany), calibrated with pure indium and zinc standards, cooling system: PerkinElmer Intracooler 2 (Solingen, Germany). An amount of 5 ± 0.1 mg of material was sealed in an aluminum pan for the analysis. Thermal history was erased with a heating scan up to 180 °C. Then, samples were cooled to 25 °C at 10 °C/min and heated again to 180 °C at 10 °C/min (second heating scan).

The degree of crystallinity ($X_c$) of neat HDPE and HDPE nanocomposites was calculated using the equation:

$$X_c = \left(\frac{\Delta H_m}{\Delta H_m^0}\right) \times \left(\frac{1}{w}\right) \quad (1)$$

where $\Delta H_m$ is the experimental heat of fusion determined from DSC, $\Delta H_m^0$ is the theoretical heat of fusion of the 100% crystalline HDPE (292.6 J/g) [27], and $w$ is the weight fraction of HDPE in the nanocomposites.

2.4.6. X-ray Diffraction Analysis (XRD)

For the analysis, nanocomposite films were prepared by compression molding at 190 °C, and then cooled at room temperature. XRD diffractograms were collected utilizing a MiniFlex II XRD system (Rigaku, Co., Tokyo, Japan) with Cu Kα radiation (0.154 nm), scanning range and rate: 5° to 50° (2θ) and 1 °/min, respectively. Crystallinity (%) was calculated according to Hay et al. [28] (Equation (2)).

$$X_c = \frac{A_c}{A_c + A_{am}} \times 100\% \quad (2)$$

where $A_{am}$ is the area of the amorphous halo and $A_c$ is the area of the crystalline peaks.

2.4.7. Polarizing Light Microscopy (PLM)

For PLM observations, a polarizing light microscope (Nikon, Tokyo, Japan, Optiphot-2), fitted with a Linkam THMS 600 heating stage, a Linkam TP 91 control unit, and a Jenoptic ProgRes C10Plus camera with the Jenoptik ProgRes® CapturePro V.2 software, were utilized. Samples were heated up to 180 °C, at 90 °C/min, kept at that temperature for three minutes to ensure that all the HDPE crystals were melted, and then cooled to room temperature (25 °C) at 10 °C/min. Spherulite images are captured at around 125 °C at magnification ×40.

2.4.8. Tensile Test

Tensile testing was conducted on a Shimadzu EZ Test Tensile Tester, Model EZ-LX (Shimadzu, Kyoto, Japan) with a 2 kN load cell and a crosshead speed of 5 mm/min, in accordance with ASTM D882 [29]. Specimens in a dumbbell shape were cut using a Wallace cutting press (central portion 5.0 × 0.5 mm thick, gauge length 22 mm). At least five measurements were conducted per sample, and the average was used to calculate the mean values of Young's modulus, tensile strength, and elongation at breakpoint.

2.4.9. Thermogravimetric Analysis (TGA)

Thermogravimetric analysis (TGA) of HDPE nanocomposites was conducted using a SETARAM SETSYS TG-DTA 16/18 instrument, and 6 ± 0.5 mg of each sample was placed in an appropriate alumina crucible, with an empty crucible serving as a reference. To account for the buoyancy effect, a blank measurement was carried out and subtracted from the experimental curve. For the kinetic analysis study [30], HDPE nanocomposites underwent heating from 25 °C to 600 °C in a flow of $N_2$ (50 mL/min). The studied heating rates were 5, 10, 15, and 20 °C/min. Sample temperature, sample mass, its first derivative, and heat flow were continuously recorded. NETZSCH Kinetics Neo software (Version 2.6.7.8) (NETZSCH, Selb, Germany) [31] was employed for the thermal degradation kinetic analysis of the HDPE nanocomposites.

The explanation of the degradation mechanism in HDPE/CaPim nanocomposites involved the determination of the degree of conversion ($\alpha$) and kinetic parameters. To achieve this, both isoconversional methods and model fitting methods were applied. Mass curves were recorded at different heating rates (5, 10, 15, and 20 °C/min) under a nitrogen atmosphere [30]. The general equation for solid-state reactions can be employed to express the rate of the (degradation) reaction:

$$\frac{da}{dt} = k(T)f(a) \quad (3)$$

In this context, $k(T)$ represents the reaction rate constant, $f(\alpha)$ stands for the reaction model, and $\alpha$ denotes the degree of conversion. The degree of conversion ($\alpha$) is defined as

the proportion of the actual mass loss at a specific temperature ($\Delta m$) to the total mass loss ($\Delta m_{tot}$), which occurs upon the completion of the degradation process.

$$\alpha = \frac{m_0 - m}{m_0 - m_f} = \frac{\Delta m}{\Delta m_{tot}} \tag{4}$$

The algebraic expression $f(\alpha)$ that constitutes the kinetic model delineates the kinetics of the solid-state reaction. The relationship between temperature and reaction rate is defined by the Arrhenius equation, $k(T) = Ae^{-E/RT}$, where $E$ represents the apparent activation energy (kJ/mol), R is the gas constant (8.314 J/mol·K), A is the pre-exponential factor ($s^{-1}$), and T is the absolute temperature (K).

Isoconversional methods are categorized into differential and integral methods, with the commonly employed ones being the differential isoconversional method by Friedman [32], the integral isoconversional method by Vyazovkin [33], and the integral isoconversional method of Ozawa, Flynn, and Wall (OFW) [34].

Friedman's differential isoconversional method:

$$\ln\left[\beta_i \left(\frac{da}{dt}\right)_{a,i}\right] = \ln[f(a)A_a] - \frac{E_a}{RT_{a,i}} \tag{5}$$

where $A$ represents the pre-exponential factor, and $\beta$ signifies the heating rate. To derive the activation energy ($E$) values for a constant conversion function, one must compute the slope of the straight lines from the plot $\ln[\beta_i(d\alpha/dt)_{\alpha,i}]$ against $1/T_{\alpha,i}$. Differential methods are advantageous as approximations are avoided and can be applied to any temperature program. However, their accuracy is constrained by a determination threshold on the baseline, and, on occasion, they may exhibit numerical instability in comparison to integral methods.

Vyazovkin has introduced an isoconversional nonlinear method aimed at calculating $E_\alpha$:

$$\Phi(E_\alpha) = \sum_{i=1}^{n} \sum_{j\neq 1}^{n} \frac{J[E_\alpha, T_i(t_\alpha)]}{J[E_\alpha, T_j(t_\alpha)]} \tag{6}$$

the indices $i$ and $j$ refer to the sets of experiments conducted under varying heating rates, $n$ represents the total number of experiments, and $J$ is assessed across small intervals of $E_\alpha$ variation:

$$J[E_\alpha, T_i(t_\alpha)] = \int_{t_{\alpha-\Delta\alpha}}^{t_\alpha} exp\left[\frac{-E_\alpha}{RT_i(t)}\right] dt \tag{7}$$

The $E_\alpha$ value is computed by identifying the minimum of the function $\Phi(E_\alpha)$ in Equation (6). For the calculation of $E_\alpha$, the time $t_{\alpha,i}$ and temperature $T_{\alpha,i}$ corresponding to selected $\alpha$ values are determined through precise interpolation using a Lagrangian algorithm for each temperature program ($i$-th).

The expression for the Ozawa, Flynn, and Wall equation can be formulated as:

$$\ln(\beta_i) = Const - 1.052\left(\frac{E_a}{RT_a}\right) \tag{8}$$

$\beta = dT/dt = const$ represents the heating rate, and the index $i$ denotes the various heating rates applied to the experimental data. The activation energy ($E_a$) values can be determined from the slope of the $\ln(\beta_i)$ versus $1/T_\alpha$ plots.

## 3. Results and Discussion

### *3.1. Synthesis and Structural Characterization of HDPE/CaPim Nanocomposites*

CaPim was synthesized by the neutralization of pimelic acid by calcium hydroxide and isolated as a white solid, after precipitation and filtration, in 78% yield. According to

DLS results, the average size of the CaPim particles was 0.63 ± 0.01 µm. In SEM analysis, platelets are observed for neat CaPim (Figure 1F). Four HDPE CaPim nanocomposites with a CaPim content ranging from 0.1% to 1% were prepared at 190 °C, by melt-mixing, which is a simple and cost-effective method. The obtained materials were white. Smooth surfaces with well distributed, round-shaped particles were observed by SEM (Figure 1A–E). Melt flow index (MFI) was measured (Table 1), and a decreasing trend in the melt viscosity of the nanocomposites is observed.

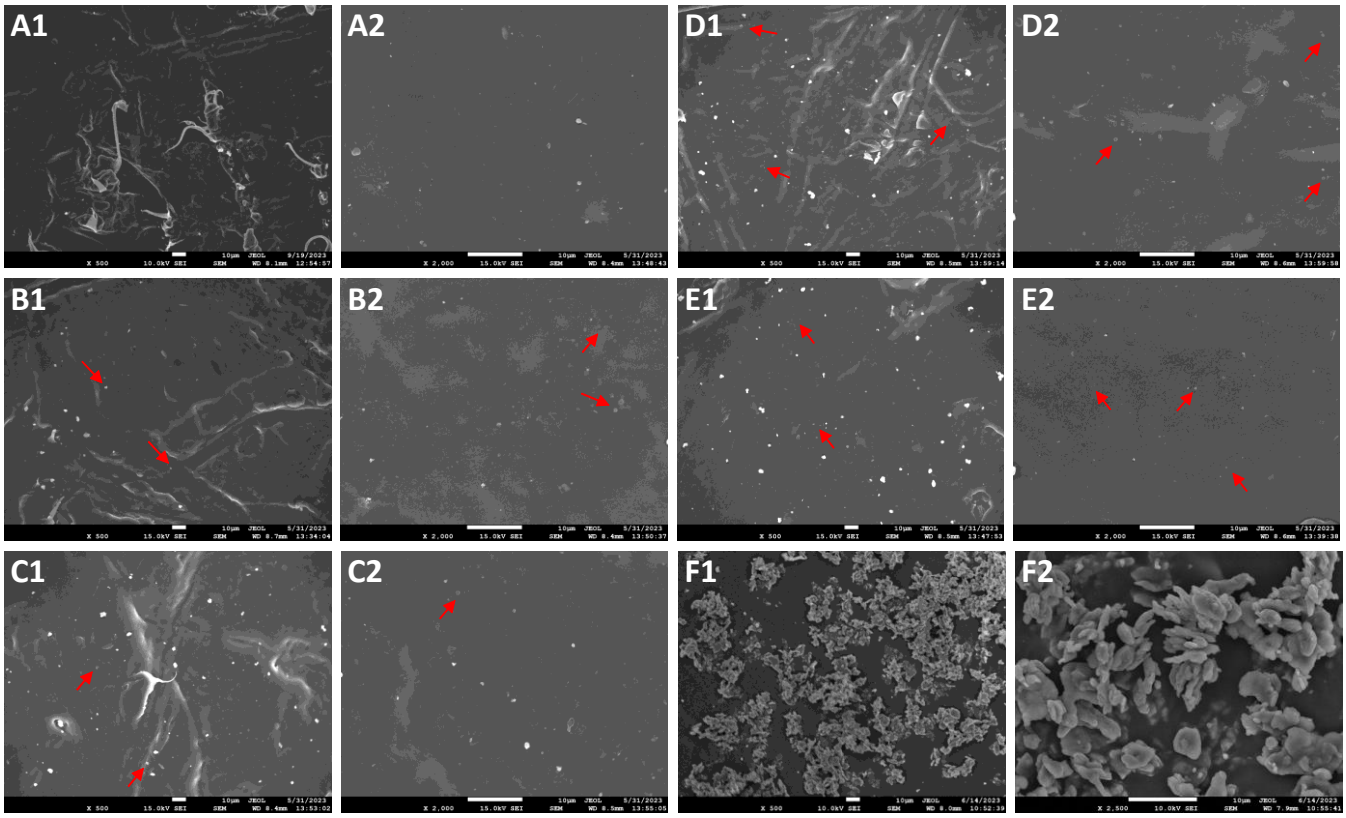


**Figure 1.** SEM photographs of CaPim and HDPE CaPim nanocomposites at different magnifications: (**A1**,**A2**) CaPim 0 (neat HDPE), (**B1**,**B2**) CaPim 0.1, (**C1**,**C2**) CaPim 0.2, (**D1**,**D2**) CaPim 0.5, (**E1**,**E2**) CaPim 1, and (**F1**,**F2**) CaPim filler. The arrows indicate CaPim particles.

The FTIR spectra of CaPim and the synthesized nanocomposites are presented in Figure 2. CaPim presents a low intensity, broad peak at 3550–3350 $cm^{-1}$ attributed to the O-H bonds of remaining humidity traces [35]. The absorbance at 2950–2850 $cm^{-1}$ arises from the C-H stretching vibration of the aliphatic chains of pimelate ion (-$(CH_2)_5$-) [36]. Very characteristically, the double peak observed at 1579 and 1540 $cm^{-1}$ can be associated with the symmetric stretching vibration of the $C(O)O^-$ group, while the absorbance detected at 1469 and 1417 $cm^{-1}$ corresponds to its asymmetric stretching vibration [35]. Regarding the nanocomposites, the main absorbance peaks are attributed to the HDPE matrix, the broad peak centered at 2900–2800 $cm^{-1}$ is attributed to the asymmetric and symmetric stretching vibrations of the C-H bonds, and the strong absorbance at 1460 $cm^{-1}$ corresponds to the $CH_2$ asymmetric changing angle vibration, while the absorbance at 720 $cm^{-1}$ arises from the $CH_2$ methylene in-plane vibration [36–38]. Due to the low CaPim content, the characteristic absorbance bands are mostly not detectable; nevertheless, when the additive content reached 0.5% and 1%, the absorbances originating from the $C(O)O^-$ group stretching vibrations of the pimelate ion were observable at 1570 and 1540 $cm^{-1}$. No specific shifting of the absorbance bands is observed; therefore, no or few interactions between CaPim and HDPE are expected.

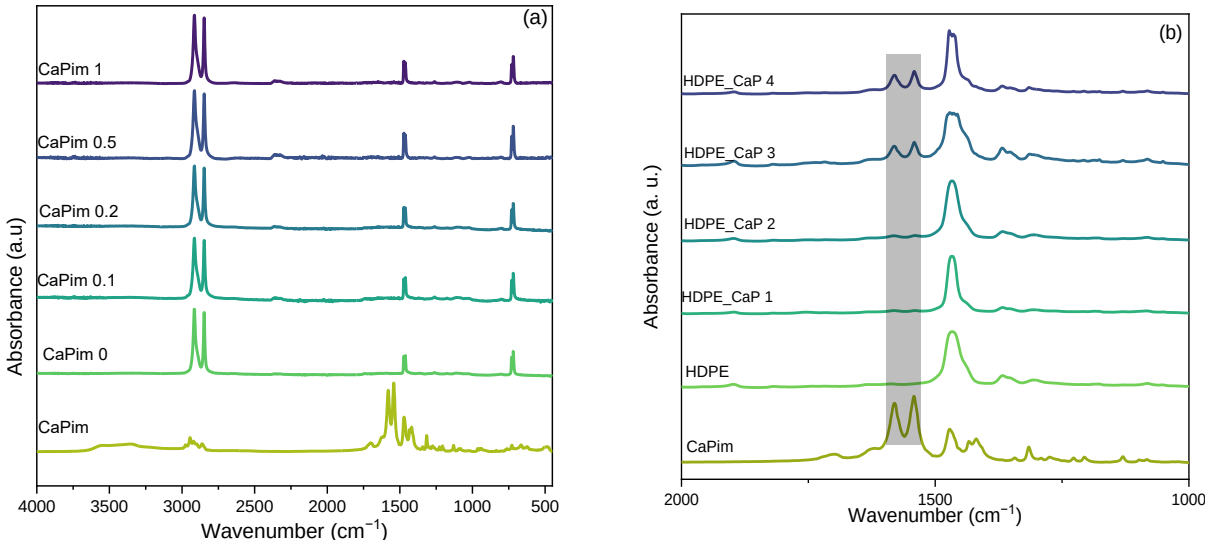


**Figure 2.** (**a**) ATR-FTIR spectra of HDPE, CaPim, and their nanocomposites and (**b**) FTIR spectra in the region of 2000–1000 cm$^{-1}$.

### *3.2. Thermal Properties and Crystallinity*

The DSC results, after erasing the thermal history, are presented in Figure 3A and Table 2. No significant shift in the melting (135 °C) and crystallization (116 °C) temperatures are observed due to the presence of CaPim. The observed uniformity in the melting temperature and crystallization temperature provides additional confirmation and substantiates the results derived from the FTIR analysis.

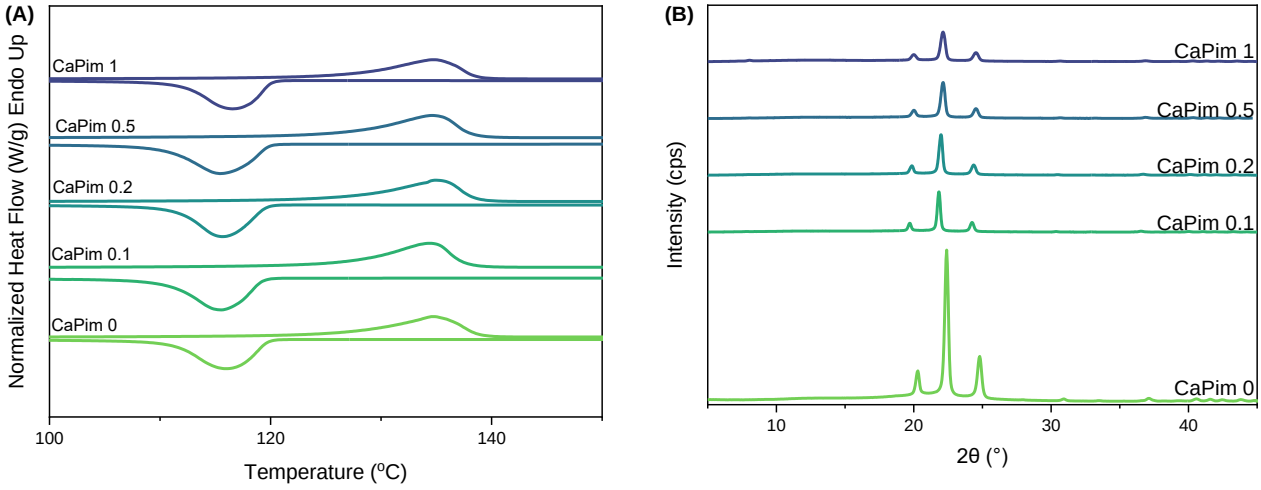


**Figure 3.** (**A**) DSC and (**B**) XRD patterns of HDPE and its nanocomposites with CaPim.

**Table 2.** DSC and XRD data of HDPE and the HDPE nanocomposites.

| Sample | Tm (°C) | Tc (°C) | ΔH (J/g) | Xc (%) DSC | Xc (%) XRD |
|---|---|---|---|---|---|
| CaPim 0 | 135.0 | 116.0 | 215.5 | 74 | 76 |
| CaPim 0.1 | 134.4 | 115.5 | 188.9 | 65 | 79 |
| CaPim 0.2 | 135.0 | 115.7 | 171.3 | 59 | 78 |
| CaPim 0.5 | 134.7 | 115.5 | 186.0 | 64 | 77 |
| CaPim 1 | 134.7 | 116.6 | 161.6 | 56 | 78 |

Regarding the XRD patterns presented below (Figure 3B), three diffraction peaks for HDPE are observed from 20° to 30°, corresponding to the orthorhombic phase, that agree

with the literature [39]. The addition of CaPim did not cause any shifts in the diffractive peaks, which indicates that the crystalline structure of HDPE is not affected by the addition of CaPim, suggesting that interactions at the molecular level do not occur [15].

The DSC calculations yielded a crystallinity value of 74%, aligning closely with the XRD results, which indicated a crystallinity of 76%. Shafiei et al. [40] determined a substantial level of crystallinity (74.23%) for neat HDPE through XRD calculations. The DSC calculations reveal a decrease in the crystallinity of the HDPE/GNPs nanocomposites in comparison to neat HDPE. However, the XRD analysis indicates an increase in crystallinity with the addition of the CaPim filler. In a previous work from our research team on HDPE graphene nanocomposites [41], higher crystallinity values were observed using XRD, likely attributed to the highly crystalline nature of graphene, while conventional DSC yielded lower values, emphasizing the necessity to consider simultaneous melting and recrystallization during heating for accurate crystallinity calculations. Conversely, XRD measurements indicated a tendency for slightly higher crystallinity values for HDPE/CaPim nanocomposites, likely attributed to the crystalline nature of CaPim.

The nanocomposites were further examined by polarizing light microscopy (PLM) and the spherulite images captured during cooling are presented below (Figure 4, 125 °C, magnification ×40). Regarding neat HDPE, well-organized spherulites are generally observed [41–44]. In the case of nanocomposites, the ones with the lowest CaPim contents exhibit few and small crystallites. As CaPim content increases, bigger crystallites are formed. In the nanocomposites with 0.5% and 1% of CaPim (Figure 4D,E), higher quality crystallites are observed compared to neat HDPE (CaPim 0).

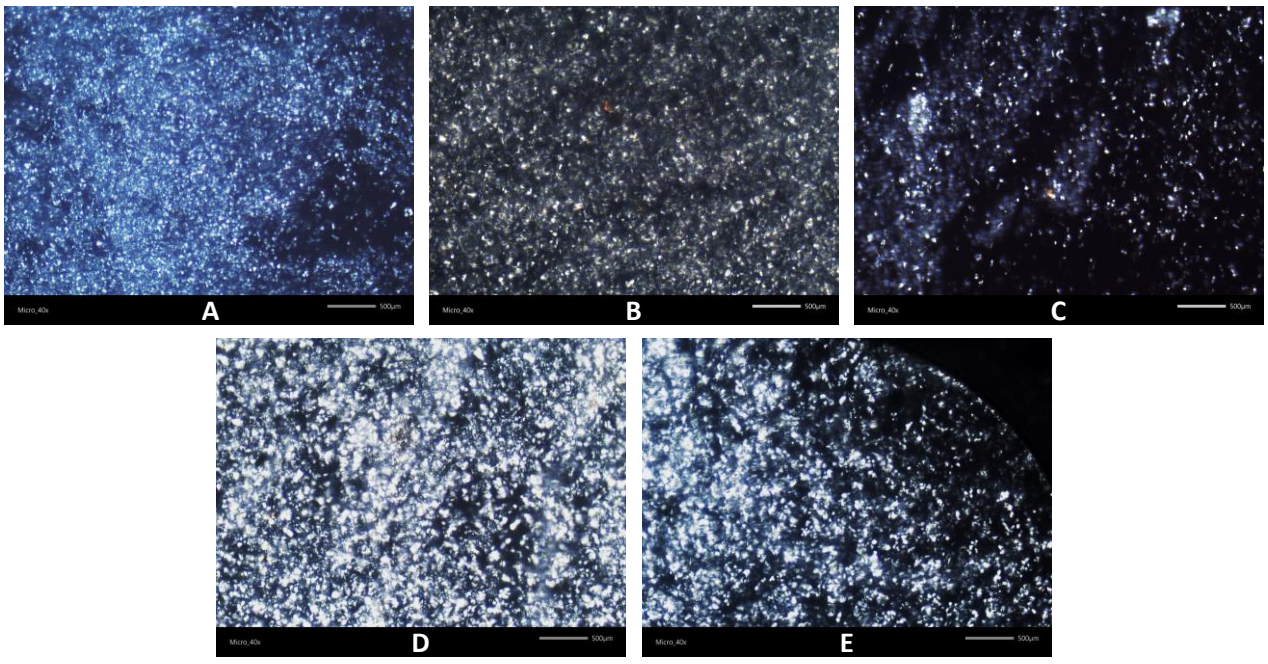


**Figure 4.** PLM images of HDPE (**A**) and its nanocomposites with 0.1–1% CaPim (**B**–**E**) at 125 °C.

Overall, it would seem that CaPim particles do not act as typical nucleating agents in the present HDPE nanocomposites. In the present study, the degree of crystallinity of the nanocomposites as calculated by DSC results is indeed lower than in neat HDPE. However, PLM observations and XRD measurements indicate the formation of bigger crystallites within a comparable timeframe, particularly evident in nanocomposites with 0.5% and 1% of CaPim. MFI measurements indicate a decreasing melt viscosity with increasing CaPim content, which could contribute to a higher chain mobility and thus would allow the formation of bigger crystallites.

### *3.3. Mechanical Behavior*

The results from the tensile test are presented in Figure 5. Stress at break and Young's modulus are retained, but elongation at break decreases compared to neat HDPE. In more detail, regarding stress at break values, while variations fall within the margin of error, results seem to suggest an increasing tendency with increasing CaPim content. This can be ascribed to the incorporation of more rigid nanoparticles in the polymer matrix. In the case of Young's modulus, a decreasing trend is observed with increasing CaPim content, but once more the differences with HDPE are small and within the margin of error. It can be said that, overall, the behavior of HDPE is retained without property loss. Finally, concerning elongation at break, CaPim 0.5 showed an improved behavior compared to the other nanocomposites, but all nanocomposites still exhibit lower performance compared to HDPE. A decrease in elongation at break is typically observed when a rigid reinforcing filler is incorporated in a polymeric matrix.

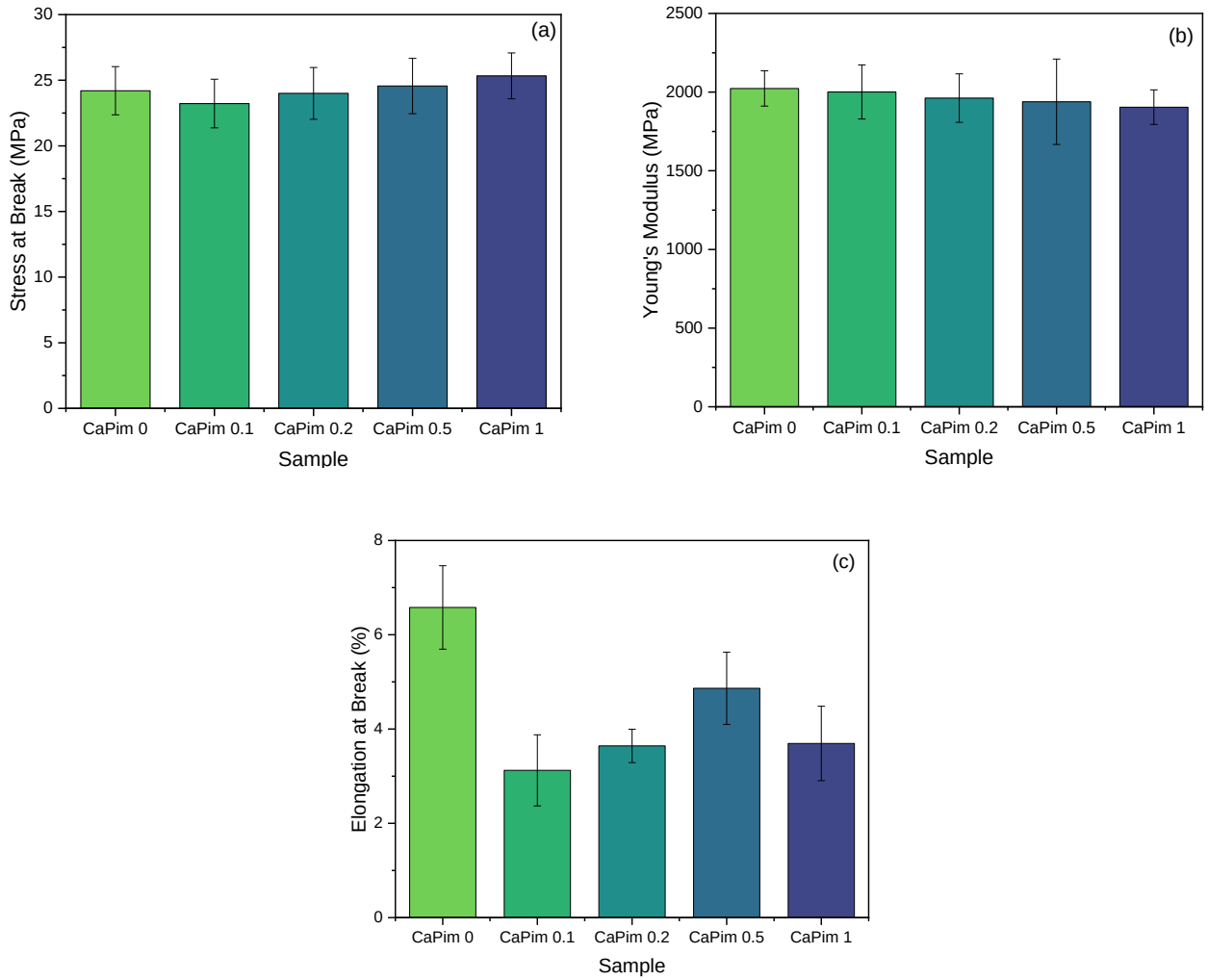


**Figure 5.** (**a**) Stress at break, (**b**) Young's modulus, (**c**) elongation at break of HDPE and its nanocomposites with CaPim.

The morphology of the fractured surfaces after tensile testing was observed by SEM (Figure 6). A smooth surface with a neat fracture is clearly observed for neat HDPE, while characteristic striations can also be observed [45]. Nanocomposites present a rougher surface with increasing filler content, and voids and cracks are increasingly detected on the failure surfaces. A more fibrillated morphology is obvious at the fracture points at low filler content, but as CaPim content increases the fibrils become shorter, suggesting a more brittle fracture.

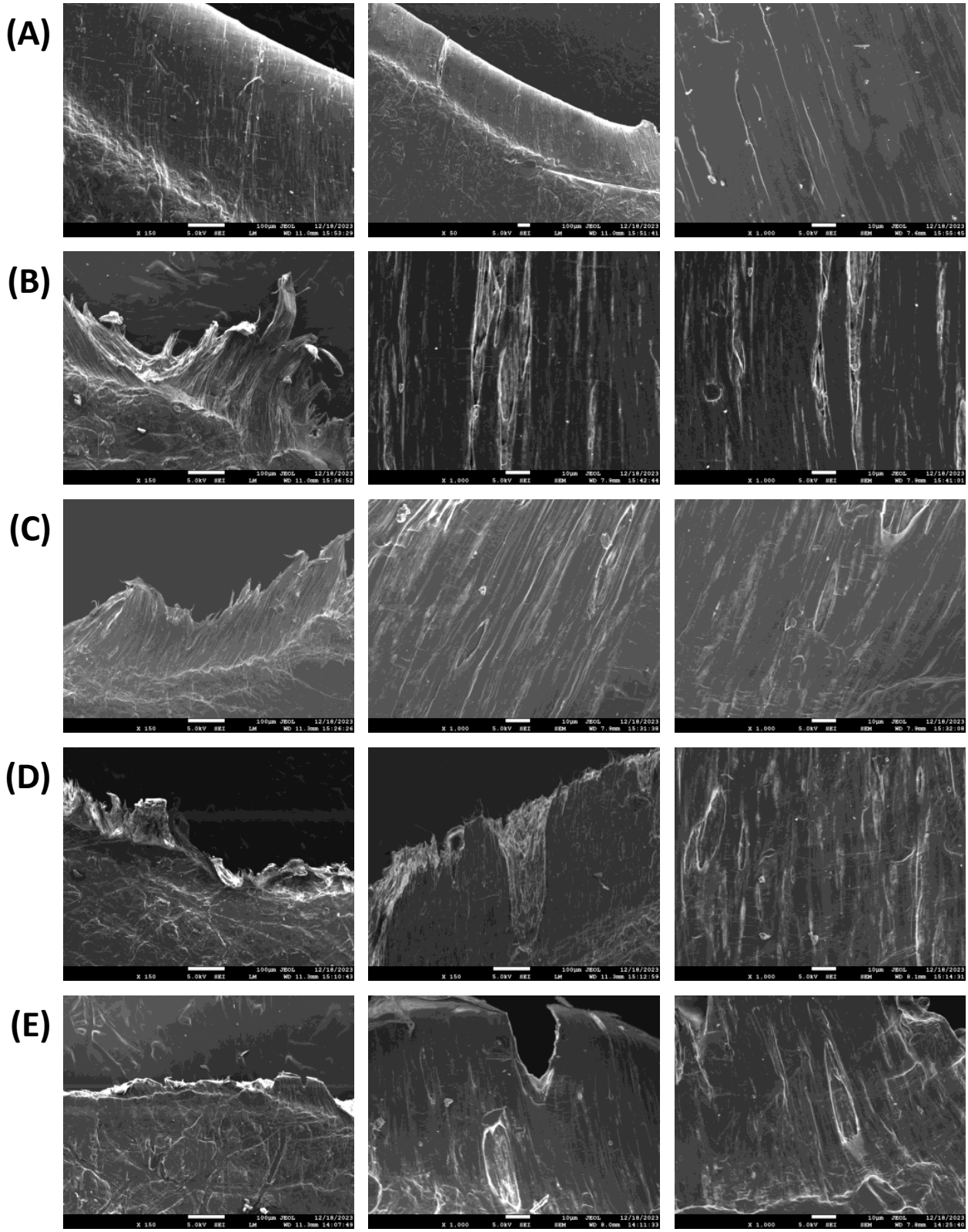


**Figure 6.** Fractured surfaces after tensile testing at two different magnifications. (**A**) Capim 0 (neat HDPE), (**B**) CaPim 0.1, (**C**) CaPim 0.2, (**D**) CaPim 0.5, and (**E**) CaPim 1.

### *3.4. Thermal Stability*

Figure 7 illustrates the TGA thermograms and dTG curves for neat HDPE, CaPim (depicted in the inset), and HDPE CaPim nanocomposites at a heating rate of 20 °C/min

under a nitrogen atmosphere. According to previous studies [46], the decomposition process of CaPim manifests in three distinct mass loss stages. The mass loss of 38.5% observed at 145–340 °C is attributed to the evaporation of crystalline-bonded water and organic molecules. The mass loss of 31.1% at 340–500 °C is associated with the evaporation of organic substances, produced by the decomposition of CaPim. The mass loss of 13.2% at 500–715 °C corresponds to the evaporation of $CO_2$ resulting from the decomposition of $CaCO_3$.

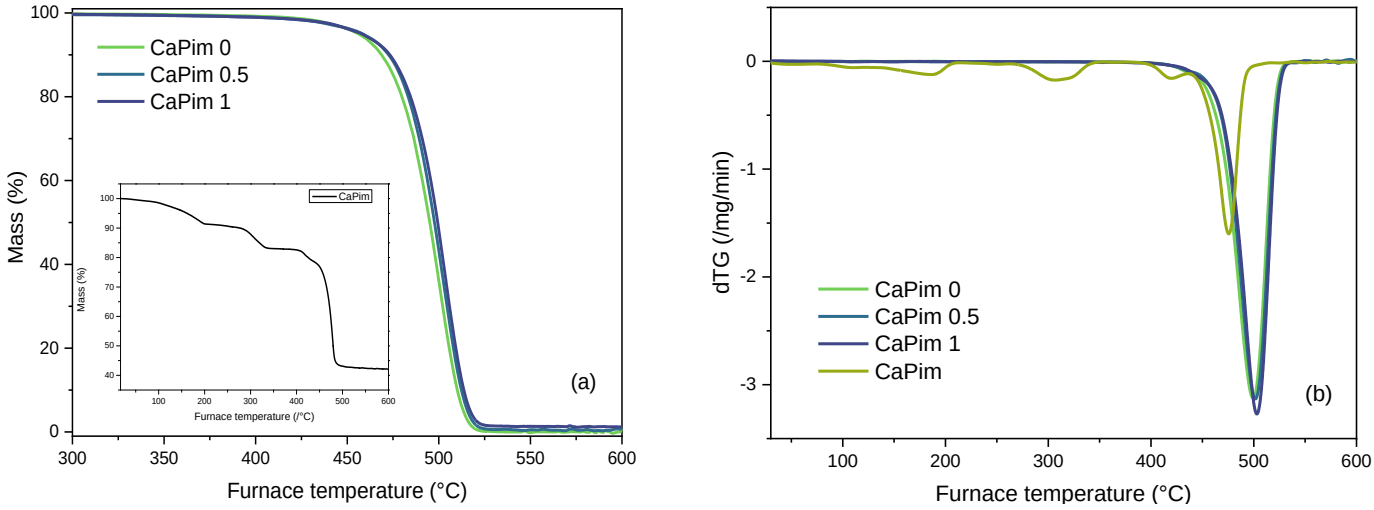


**Figure 7.** (**a**) TGA and (**b**) dTG curves of CaPim-filled HDPE nanocomposites heated at a rate of 20 °C/min in a nitrogen environment.

The TGA curves reveal that both neat HDPE and HDPE CaPim nanocomposites exhibit commendable thermostability, displaying no significant mass loss until 400 °C. Table 3 lists the specific temperatures for 2.5% and 5% mass loss for each HDPE nanocomposite. The maximum thermal degradation temperatures ($T_{d,max}$) of HDPE CaPim nanocomposites were increased, indicating a notable improvement in their thermal stability. When the amount of CaPim in the HDPE nanocomposites increases, so does the residual level at 600 °C. It is notable that the CaPim 1 nanocomposite shows the highest rate of breakdown at 503.1 °C when the dTG curves are analyzed.

**Table 3.** TGA results of studied samples. $T_{2.5}$ and $T_5$ are the temperatures where 2.5% and 5% mass loss are observed. $T_{d,max}$ is the temperature where the maximum degradation rate is reached.

| Sample | $T_{2.5}$ (°C) | $T_5$ (°C) | $T_{d,max}$ (°C) |
|---|---|---|---|
| CaPim 0 | 438.5 | 456.2 | 499.4 |
| CaPim 0.5 | 439.1 | 457.4 | 501.6 |
| CaPim 1 | 440.0 | 457.9 | 503.1 |

Three iso-conversional approaches, including Friedman's differential isoconversional method, Vyazovkin's integral isoconversional method, and OFW's integral isoconversional method, were utilized to compute activation energies [30,31,44,45,47]. Figure 8 illustrates the $E_\alpha$ values for CaPim 0.5 and CaPim 1 nanocomposites across the degree of conversion $\alpha$, employing the aforementioned isoconversional methods. The values calculated using the Friedman approach and the mean $E_\alpha$ value derived from the TGA curves using the Vyazovkin method match up nicely. The dependence of $E_\alpha$ in all cases points to a complex thermal degradation mechanism wherein the early and late stages of degradation kinetics are regulated by distinct processes. In the first region, the $E_\alpha$ values for CaPim 0.5 and CaPim 1 nanocomposites exhibit an increase, while they remain nearly constant for higher

values. The mean $E_\alpha$ values for CaPim 0.5 for $\alpha < 0.2$ were determined as 203.1, 202.9, and 208.3 kJ/mol, respectively, based on the Friedman method, Vyazovkin analysis, and OFW method. Meanwhile, for $\alpha > 0.2$, these values were 222.1, 228.0, and 226.3 kJ/mol. Furthermore, the $E_\alpha$ values for the CaPim 1 nanocomposite ($\alpha < 0.2$) were found to be 208.5, 205.7, and 211.0 kJ/mol for the Friedman method, Vyazovkin analysis, and OFW method, respectively. For $\alpha > 0.1$, these values were 235.5, 240.3, and 237.3 kJ/mol. Notably, the CaPim 0.5 nanocomposite exhibits a lower activation energy than CaPim 1, indicating that it requires less activation energy for thermal degradation.

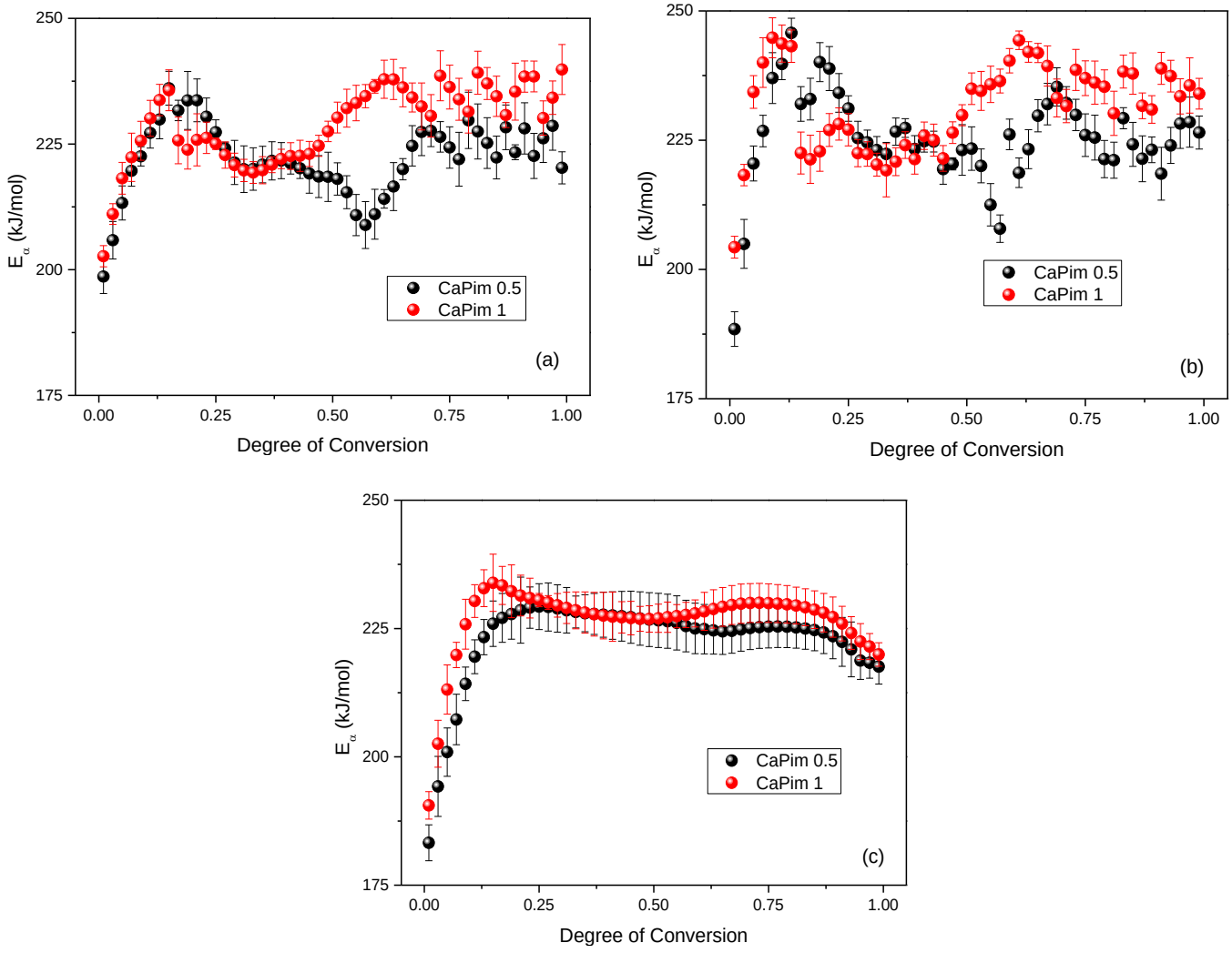


**Figure 8.** The relationship between $E_\alpha$ and $\alpha$ for CaPim 0.5 and CaPim 1 nanocomposites as determined by three methods: (**a**) Friedman, (**b**) Vyazovkin, and (**c**) OFW methods.

The model-fitting procedure, which is also referred to as multivariate non-linear regression, was utilized to ascertain the kinetic triplet and the degradation mechanism for every reaction. This involved comparing the experimental data (across four heating rates) with theoretical data. Initially, it was believed that a single-step reaction mechanism would be responsible for the significant mass loss. When there was an inadequate match with the experimental data, two or more mechanisms were combined. In an earlier study [48], we determined that, for neat HDPE, the optimal fitting between the experimental and theoretical results (correlation coefficient of at least 0.9998) is obtained through a combination of the nth-order reaction mechanism (Fn), $f(\alpha) = (1 - \alpha)^n$, with the mechanism of autocatalysis n-order (Cn), $f(\alpha) = (1 - \alpha)^n(1 + K_{cat}X)$, where $K_{cat}$ is the autocatalysis rate constant and $X$ the extent of conversion of the autocatalytic reactions. The first degradation mechanism

corresponds to a small mass loss, while the main mass loss is associated to the second degradation mechanism. The combination of Fn–Cn reaction models fits the experimental data of CaPim 0.5 and CaPim 1 nanocomposites quite well (Figure 9). The values of the correlation coefficients ($R^2$) were 0.99982 and 0.99980 for CaPim 0.5 and CaPim 1 nanocomposites, respectively. As a result, there are two phases to the degradation of the two samples under study: the primary stage of degradation happens at higher temperatures, while the first stage corresponds to a very minor mass loss. Table 4 provides a summary of the computed parameters derived from the tested models. The $E_\alpha$ values determined by isoconversional methods, and the two-step mechanism model's computations agree well (Figure 9). The effect of CaPim filler is pronounced, increasing the activation energy of thermal degradation in agreement with the calculated dependence of E on α and the thermal stability enhancement of the HDPE matrix (Figure 7). The pre-exponential factor of CaPim 1 presents a slightly higher value than those of the CaPim 0.5 nanocomposite, in accordance with the calculated E values. This means that the rate constant of the CaPim 0.5 nanocomposite is larger, accelerating the thermal degradation.

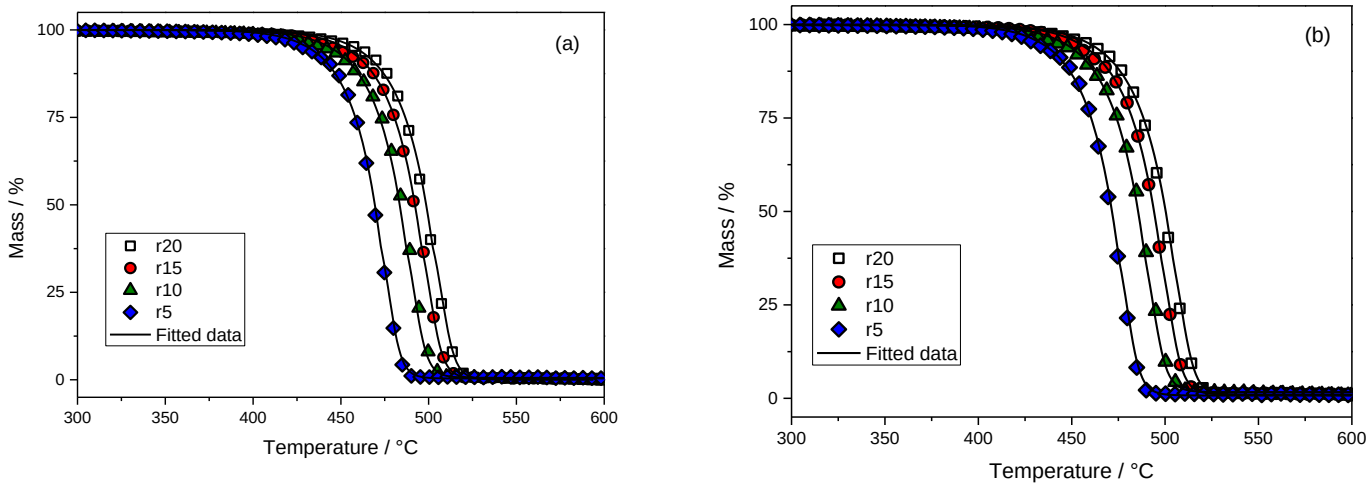


**Figure 9.** Mass (%) curves of (**a**) CaPim 0.5 and (**b**) CaPim 1 nanocomposites (symbols) and the corresponding fitting curves with the combination of Fn–Cn reaction models (continuous black lines).

**Table 4.** Activation energy, pre-exponential factor, and reaction order (n) of HDPE/CaPim nanocomposites.

| Sample | Model | $E_\alpha$ /kJmol$^{-1}$ | log$A_1$/s$^{-1}$ | n | Log $K_{cat}$ | Contribution | $R^2$ |
|---|---|---|---|---|---|---|---|
| CaPim 0.5 | Fn | 204.1 | 10.183 | 0.168 | - | 0.258 | 0.99982 |
| | Cn | 223.7 | 11.738 | 0.778 | 1.065 | 0.742 | |
| CaPim 1 | Fn | 210.5 | 10.934 | 0.231 | - | 0.299 | 0.99980 |
| | Cn | 236.6 | 11.956 | 0.781 | 1.073 | 0.701 | |

## 4. Conclusions

A series of HDPE nanocomposites with nanosized CaPim filler were prepared by melt-mixing with CaPim content ranging from 0.1% to 1%, and the effect of the incorporation of the filler into the polymer matrix was studied. The thermal transitions and crystal structure of HDPE are not significantly affected by the incorporation of CaPim. PLM observations evidenced the formation of larger crystallites with increasing CaPim content. Mechanical properties are retained overall. Interestingly, a higher thermal stability is observed with increasing CaPim content. Isoconversional results depicted a complex degradation mechanism, with distinct processes influencing the early and late stages of degradation kinetics. CaPim 0.5 exhibited lower activation energy than CaPim 1, indicating its lower energy requirement for thermal degradation. Model-fitting analysis further confirmed a two-step

degradation mechanism for the nanocomposites, combining nth-order and autocatalysis mechanisms. The present work is a preliminary study on HDPE/CaPim nanocomposites. More in-depth studies are in progress, including notably fast scanning calorimetry experiments to obtain more insights on the effect of CaPim on HDPE crystallization.

**Author Contributions:** Conceptualization, K.C. and D.N.B.; investigation, C.S., D.K., E.T. and A.Z.; writing—original draft preparation, C.S., E.T. and A.Z.; writing—review and editing, K.C. and D.N.B.; supervision, D.N.B.; funding acquisition, D.N.B. All authors have read and agreed to the published version of the manuscript.

**Funding:** This research was funded by the European Union's Horizon Europe Framework Programme under Grant Agreement No. 101058449.

**Data Availability Statement:** Data is available upon request.

**Acknowledgments:** This project has received funding from the European Union's Horizon Europe Framework Programme under Grant Agreement No. 101058449. Views and opinions expressed are, however, those of the author(s) only and do not necessarily reflect those of the European Union or HADEA. Neither the European Union nor the granting authority can be held responsible for them.

**Conflicts of Interest:** The authors declare no conflicts of interest.

## References

1. Olesik, P.; Godzierz, M.; Kozioł, M.; Jała, J.; Szeluga, U.; Myalski, J. Structure and Mechanical Properties of High-Density Polyethylene Composites Reinforced with Glassy Carbon. *Materials* **2021**, *14*, 4024. [CrossRef]
2. Awad, A.H.; El Gamasy, R.; El Wahab, A.A.; Abdellatif, M.H. Mechanical and Physical Properties of PP and HDPE. *Eng. Sci.* **2019**, *4*, 34–42. [CrossRef]
3. Arshad, M. Kinetics of Crystallization Mechanisms in High Density Polyethylene and Isotactic Polypropylene. *Polym. Sci. Ser. A* **2021**, *63*, S23–S33. [CrossRef]
4. Chew, S.; Griffiths, J.R.; Stachurski, Z.H. The Crystallization Kinetics of Polyethylene under Isothermal and Non-Isothermal Conditions. *Polymer* **1989**, *30*, 874–881. [CrossRef]
5. Shan, H.; Lickfield, G.C. Crystallization Kinetics Study of Polyethylene. *Int. J. Polym. Anal. Charact.* **2007**, *12*, 327–338. [CrossRef]
6. Seven, K.M.; Cogen, J.M.; Gilchrist, J.F. Nucleating agents for high-density polyethylene—A review. *Polym. Eng. Sci.* **2016**, *56*, 541–554. [CrossRef]
7. Lin, Y.; Bilotti, E.; Bastiaansen, C.W.M.; Peijs, T. Transparent Semi-Crystalline Polymeric Materials and Their Nanocomposites: A Review. *Polym. Eng. Sci.* **2020**, *60*, 2351–2376. [CrossRef]
8. Paszkiewicz, S.; Pypeć, K.; Irska, I.; Piesowicz, E. Functional Polymer Hybrid Nanocomposites Based on Polyolefins: A Review. *Processes* **2020**, *8*, 1475. [CrossRef]
9. Zare, Y. Recent progress on preparation and properties of nanocomposites from recycled polymers: A review. *Waste Manag.* **2013**, *33*, 598–604. [CrossRef]
10. Kane, S.; Van Roijen, E.; Ryan, C.; Miller, S. Reducing the Environmental Impacts of Plastics While Increasing Strength: Biochar Fillers in Biodegradable, Recycled, and Fossil-Fuel Derived Plastics. *Compos. Part C Open Access* **2022**, *8*, 100253. [CrossRef]
11. Sathishkumar, T.P.; Navaneethakrishnan, P.; Shankar, S.; Rajasekar, R.; Rajini, N. Characterization of Natural Fiber and Composites—A Review. *J. Reinf. Plast. Compos.* **2013**, *32*, 1457–1476. [CrossRef]
12. Dunlop, M.J.; Bissessur, R. Nanocomposites based on graphene analogous materials and conducting polymers: A review. *J. Mater. Sci.* **2020**, *55*, 6721–6753. [CrossRef]
13. Paul, D.R.; Robeson, L.M. Polymer nanotechnology: Nanocomposites. *Polymer* **2008**, *49*, 3187–3204. [CrossRef]
14. Pleşa, I.; Noţingher, P.V.; Stancu, C.; Wiesbrock, F.; Schlögl, S. Polyethylene Nanocomposites for Power Cable Insulations. *Polymers* **2018**, *11*, 24. [CrossRef]
15. Wang, S.; Zhang, J. Non-isothermal crystallization kinetics of high density polyethylene/titanium dioxide composites via melt blending. *J. Therm. Anal. Calorim.* **2014**, *115*, 63–71. [CrossRef]
16. Miao, W.; Zhu, H.; Duan, T.; Chen, H.; Wu, F.; Jiang, L.; Wang, Z. High-density polyethylene crystals with double melting peaks induced by ultra-high-molecular-weight polyethylene fibre. *R. Soc. Open Sci.* **2018**, *5*, 180394. [CrossRef]
17. Papageorgiou, D.G.; Chrissafis, K.; Bikiaris, D.N. β-Nucleated Polypropylene: Processing, Properties and Nanocomposites. *Polym. Rev.* **2015**, *55*, 596–629. [CrossRef]
18. Yue, Y.; Hu, D.; Zhang, Q.; Lin, J.; Feng, J. The effect of structure evolution upon heat treatment on the beta-nucleating ability of calcium pimelate in isotactic polypropylene. *Polymer* **2018**, *149*, 55–64. [CrossRef]
19. Papageorgiou, D.G.; Vourlias, G.; Bikiaris, D.N.; Chrissafis, K. Synergistic Effect of Functionalized Silica Nanoparticles and a β-Nucleating Agent for the Improvement of the Mechanical Properties of a Propylene/Ethylene Random Copolymer. *Macromol. Mater. Eng.* **2014**, *299*, 707–721. [CrossRef]

20. Zhang, Y.F.; Lin, X.F.; Chen, S. Preparation and nucleation effect of a novel compound nucleating agent carboxylated graphene/calcium pimelate for isotactic polypropylene. *J. Therm. Anal. Calorim.* **2019**, *136*, 2363–2371. [CrossRef]
21. González, A.; Pérez, E.; Almendarez, A.; Villegas, A.; Vallejo-Montesinos, J. Calcium pimelate supported on $TiO_2$ nanoparticles as isotactic polypropylene prodegradant. *Polym. Bull.* **2016**, *73*, 39–51. [CrossRef]
22. Tanniru, M.; Misra, R.D.K.; Berbrand, K.; Murphy, D. The determining role of calcium carbonate on surface deformation during scratching of calcium carbonate-reinforced polyethylene composites. *Mater. Sci. Eng. A* **2005**, *404*, 208–220. [CrossRef]
23. Awan, M.O.; Shakoor, A.; Rehan, M.S.; Gill, Y.Q. Development of HDPE composites with improved mechanical properties using calcium carbonate and NanoClay. *Phys. B Condens. Matter* **2021**, *606*, 412568. [CrossRef]
24. Sepet, H.; Aydemir, B.; Tarakcioglu, N. Evaluation of mechanical and thermal properties and creep behavior of micro- and nano-CaCO3 particle-filled HDPE nano- and microcomposites produced in large scale. *Polym. Bull.* **2020**, *77*, 3677–3695. [CrossRef]
25. *ASTM D1238-10*; Standard Test Method for Melt Flow Rates of Thermoplastics by Extrusion Plastometer. ASTM International: West Conshohocken, PA, USA, 2010.
26. *ISO 1133-1:2022*; Plastics Determination of the Melt Mass-Flow Rate (MFR) and Melt Volume-Flow Rate (MVR) of Thermoplastics. ISO (The International Organization for Standardization): Geneva, Switzerland, 2022.
27. Awad, A.H.; El-Wahab, A.A.A.; El-Gamsy, R.; Abdel-latif, M.H. A study of some thermal and mechanical properties of HDPE blend with marble and granite dust. *Ain Shams Eng. J.* **2019**, *10*, 353–358. [CrossRef]
28. Lu, X.F.; Hay, J.N. Isothermal crystallization kinetics and melting behaviour of poly(ethylene terephthalate). *Polymer* **2001**, *42*, 9423–9431. [CrossRef]
29. *ASTM D882-18*; Standard Test Method for Tensile Properties of Thin Plastic Sheeting. ASTM International: West Conshohocken, PA, USA, 2018.
30. Vyazovkin, S.; Burnham, A.K.; Criado, J.M.; Pérez-Maqueda, L.A.; Popescu, C.; Sbirrazzuoli, N. ICTAC Kinetics Committee recommendations for performing kinetic computations on thermal analysis data. *Thermochim. Acta* **2011**, *520*, 1–19. [CrossRef]
31. Kinetics Neo. Available online: https://kinetics.netzsch.com/ (accessed on 20 December 2023).
32. Friedman, H.L. Kinetics of thermal degradation of char-forming plastics from thermogravimetry. Application to a phenolic plastic. *J. Polym. Sci. Part C Polym. Symp.* **1964**, *6*, 183–195. [CrossRef]
33. Vyazovkin, S. Evaluation of Activation Energy of Thermally Stimulated Solid-State Reactions under Arbitrary Variation of Temperature. *J. Comput. Chem.* **1997**, *18*, 393–402. [CrossRef]
34. Ozawa, T. Kinetics of non-isothermal crystallization. *Polymer* **1971**, *12*, 150–158. [CrossRef]
35. Li, X.; Hu, K.; Ji, M.; Huang, Y.; Zhou, G. Calcium dicarboxylates nucleation of β-polypropylene. *J. Appl. Polym. Sci.* **2002**, *86*, 633–638. [CrossRef]
36. Meng, M.R.; Dou, Q. Effect of Filler Treatment on Crystallization, Morphology and Mechanical Properties of Polypropylene/Calcium Carbonate Composites. *J. Macromol. Sci.* **2009**, *48*, 213–225. [CrossRef]
37. Fávaro, S.L.; Rubira, A.F.; Muniz, E.C.; Radovanovic, E. Surface modification of HDPE, PP, and PET films with $KMnO_4$/HCl solutions. *Polym. Degrad. Stab.* **2007**, *92*, 1219–1226. [CrossRef]
38. Jung, M.R.; Horgen, F.D.; Orski, S.V.; Rodriguez C., V.; Beers, K.L.; Balazs, G.H.; Jones, T.T.; Work, T.M.; Brignac, K.C.; Royer, S.-J.; et al. Validation of ATR FT-IR to identify polymers of plastic marine debris, including those ingested by marine organisms. *Mar. Pollut. Bull.* **2018**, *127*, 704–716. [CrossRef]
39. Sutar, H.; Murmu, R.; Dutta, C.; Ozcan, M.; Mishra, S.C. High Density Polyethylene (HDPE) and Polypropylene (PP) Polyblend: An Experimental Approach. In *New Advances in Materials Science and Engineering*; Goel, A.K., Ed.; Book Publisher International: West Bengal, India, 2019; p. 1. ISBN 978-9-3892-4626-1.
40. Shafiei, M.; Ghasemi, I.; Gomari, S.; Abedini, A.; Jamjah, R. Positive Temperature Coefficient and Electrical Conductivity Investigation of Hybrid Nanocomposites Based on High-Density Polyethylene/Graphene Nanoplatelets/Carbon Black. *Phys. Status Solidi* **2021**, *218*, 2100361. [CrossRef]
41. Tarani, E.; Arvanitidis, I.; Christofilos, D.; Bikiaris, D.N.; Chrissafis, K.; Vourlias, G. Calculation of the degree of crystallinity of HDPE/GNPs nanocomposites by using various experimental techniques: A comparative study. *J. Mater. Sci.* **2023**, *58*, 1621–1639. [CrossRef]
42. Sahoo, P.C.; Murmu, R.; Patra, S.C.; Dutta, C.; Sutar, H. Electrical Behaviour and Spherulites Morphology of HDPE/PP Polyblends with HDPE as Base Material. *Mater. Sci. Appl.* **2018**, *9*, 837–843. [CrossRef]
43. Fu, Q.; Men, Y.; Strobl, G. Understanding of the tensile deformation in HDPE/LDPE blends based on their crystal structure and phase morphology. *Polymer* **2003**, *44*, 1927–1933. [CrossRef]
44. Huang, J.W.; Wen, Y.L.; Kang, C.C.; Tseng, W.J.; Yen, M.Y. Nonisothermal crystallization of high density polyethylene and nanoscale calcium carbonate composites. *Polym. Eng. Sci.* **2008**, *48*, 1268–1278. [CrossRef]
45. Tarani, E.; Chrysafi, I.; Kállay-Menyhárd, A.; Pavlidou, E.; Kehagias, T.; Bikiaris, D.N.; Vourlias, G.; Chrissafis, K. Influence of Graphene Platelet Aspect Ratio on the Mechanical Properties of HDPE Nanocomposites: Microscopic Observation and Micromechanical Modeling. *Polymer* **2020**, *12*, 1719. [CrossRef] [PubMed]
46. Zhang, Y.F.; Lin, X.F.; Hu, H. Combined effect of chemically compound graphene oxide-calcium pimelate on crystallization behavior, morphology and mechanical properties of isotactic polypropylene. *Polym. Adv. Technol.* **2020**, *31*, 2301–2311. [CrossRef]

47. Budrugeac, P.; Segal, E.; Pérez-Maqueda, L.A.; Criado, J.M. The use of the IKP method for evaluating the kinetic parameters and the conversion function of the thermal dehydrochlorination of PVC from non-isothermal data. *Polym. Degrad. Stab.* **2004**, *84*, 311–320. [CrossRef]
48. Tarani, E.; Terzopoulou, Z.; Bikiaris, D.N.; Kyratsi, T.; Chrissafis, K.; Vourlias, G. Thermal conductivity and degradation behavior of HDPE/graphene nanocomposites: Pyrolysis, kinetics and mechanism. *J. Therm. Anal. Calorim.* **2017**, *129*, 1715–1726. [CrossRef]